



Detection and prediction of land use/land cover change using spatiotemporal data fusion and the Cellular Automata–Markov model

Yuting Lu · Penghai Wu · Xiaoshuang Ma · Xinghua Li

Received: 10 August 2018 / Accepted: 3 January 2019 / Published online: 14 January 2019
© Springer Nature Switzerland AG 2019

Abstract The detection and prediction of land use/land cover (LULC) change is crucial for guiding land resource management, planning, and sustainable development. In the view of seasonal rhythm and phenological effect, detection and prediction would benefit greatly from LULC maps of the same seasons for different years. However, due to frequent cloudiness contamination, it is difficult to obtain same-season LULC maps when using existing remote sensing images. This study utilized the spatiotemporal data fusion (STF) method to obtain summer Landsat-scale images in Hefei over the past 30 years. The Cellular Automata–Markov model

was applied to simulate and predict future LULC maps. The results demonstrate the following: (1) the STF method can generate the same inter-annual interval summer Landsat-scale data for analyzing LULC change; (2) the fused data can improve the LULC detection and prediction accuracy by shortening the inter-annual interval, and also obtain LULC prediction results for a specific year; (3) the areas of cultivated land, water, and vegetation decreased by 33.14%, 2.03%, and 16.36%, respectively, and the area of construction land increased by 200.46% from 1987 to 2032. The urban expansion rate will reach its peak until 2020, and then slow down. The findings provide valuable information for urban planners to achieve sustainable development goals.

Y. Lu · P. Wu · X. Ma
School of Resources and Environmental Engineering, Anhui University, Hefei 230601 Anhui, China

Y. Lu
e-mail: luyutinglyt@163.com

X. Ma
e-mail: mxs.88@163.com

Y. Lu · P. Wu
Anhui Province Key Laboratory of Wetland Ecosystem Protection and Restoration, Anhui University, Hefei 230601 Anhui, China

P. Wu (✉)
Institute of Physical Science and Information Technology, Anhui University, Hefei 230601 Anhui, China
e-mail: wuph@ahu.edu.cn

X. Li
School of Remote Sensing and Information Engineering, Wuhan University, Wuhan 430079 Hubei, China
e-mail: lixinghua5540@whu.edu.cn

Keywords Land use and land cover · Spatiotemporal data fusion · ESTARFM · CA–Markov · Prediction

Introduction

Land use and land cover (LULC) change directly reflects on the utilization of land resources in a region, and it is also one of the key factors affecting the ecological environment (Saleem et al. 2018). LULC change involving human factors, such as the overexploitation of forests, agricultural loss, and urbanization, has caused not only natural resource shortages, but also widespread and irreversible losses of biodiversity across the globe (Bounoua et al. 2018; Pickard et al. 2017). It has become a hot issue in the study of globalization and sustainable

development (Blecic et al. 2013; Alqurashi et al. 2016). Space–time prediction and quantitative analysis of urban land use dynamics are effective ways to improve the understanding of the evolution of urban LULC change (Mas et al. 2014). Of all the numerous data, remote sensing data is regarded as the cornerstone of LULC detection and prediction.

Background

Remote sensing has tremendous potential in land resource management, due to its low cost and long time series data acquisition capability over a large spatial extent (Chandra et al. 2003). A large number of studies on LULC changes have been carried out by using remote sensing data sets (Halmy et al. 2015), such as MODIS (Alhamdan et al. 2017), Landsat (Chen et al. 2013a, b; Osgouei and Kaya 2017), and SPOT (McCarthy et al. 2018). Landsat has gradually become the first choice of LULC change research because of its convenient access, long time series, high spatial resolution, and free access features. Spatially fine analyses have been achieved by the use of Landsat, such as the spatiotemporal evolution research of LULC change (Behera 2007), urbanization (Fu and Weng 2016), vegetation coverage (Liu et al. 2017a, b), and flood mapping (Mueller et al. 2016; Mohammadi et al. 2017). In recent years, the Landsat series of satellites has been the foremost data source for the spatiotemporal detection of LULC change and LULC prediction. Long-term, high temporal frequency remotely sensed data are very important for the monitoring and analysis of LULC change, which can help us to more intuitively understand the evolutionary mechanism of LULC change, and help decision-makers to formulate and implement reasonable land use policies (Chen et al. 2008; Chen et al. 2013a, b). Ideally, all images should be collected in the same season, preferably in summer, where phenological variations are less evident, which is beneficial for extracting features of LULC (Gounaris et al. 2018; Walsh et al. 2001). However, due to the influence of cloud cover, the Landsat/ETM+ SLC-off problem after 2003, and a poor temporal resolution, it is often difficult to obtain same-season Landsat images for consecutive years. Most existing studies of long-term LULC change research have to use a few available, but not ideal, remotely sensed images (Adami et al. 2012; Prenzel 2004). The use of “bad” data can lead to great uncertainties when drawing conclusions (Mizuochi et al.

2017). How to obtain long-term and summer Landsat data for LULC research is an essential issue (Sinha et al. 2012). To solve this problem, a spatiotemporal data fusion (STF) technique was employed to fuse high temporal (but low spatial) resolution satellite data (such as MODIS) with high spatial (but low temporal) resolution satellite data (such as Landsat) to generate high spatiotemporal resolution data for the missing periods (Gao et al. 2006).

Many scholars have done a great deal of work in STF, and have obtained many research results, including a spatiotemporal adaptive reflectance fusion model (STARFM) (Gao et al. 2006) and an enhanced STARFM (ESTARFM) (Zhu et al. 2010). The fusion of biophysical parameters, such as reflectance (Gao et al. 2006; Zhu et al. 2010), land surface temperature (Wu et al. 2015), and evapotranspiration (Cammalleri et al. 2014), has greatly promoted the application of the STF method in the fields of the land cover map (Li et al. 2017), flood monitoring (Zhang et al. 2014), agriculture (Dong et al. 2016; Gao et al. 2017), the spread of infectious diseases (Liu and Weng 2012), and urban heat islands (Shen et al. 2016). However, there is little relevant research on applying STF technology onto the spatiotemporal detection of LULC change and LULC prediction. Therefore, we summarize our contributions as follows:

- An STF technique is introduced to the LULC change study, which improves the consistency and comparability of the data used.
- The summer but not annual urban LULC maps are generated, to reduce the effect of the seasonal rhythm and the phenological variations for the LULC detection and prediction analysis.
- A more accurate LULC prediction for any specific year can be achieved by using fused data.

Objectives

The main objectives of this paper are (1) to solve the spatiotemporal discontinuities in remote sensing data for the LULC change analysis; (2) to generate summer Landsat-like data for the LULC change analysis every 5 years from 1987 to 2017; (3) to explore whether the STF method is effective in LULC detection and prediction, through an accuracy analysis between the actual remote sensing data and the fused remote sensing data, then based on this, the variation characteristics of the

LULC prediction accuracy at different inter-annual intervals are investigated; and (4) to predict the spatiotemporal dynamics of future LULC change processes.

Study area and data

Study area

The Hefei metropolis, located between the latitudes 31° 30' and 32° 38' N and between the longitudes 116° 41' and 117° 53' E (as shown in Fig. 1), was chosen as the study area for this research. It belongs to a warm temperate to subtropical transitional climate type of the humid subtropical monsoon climate. The city has an annual average temperature of 15.7 °C and the rainfall is approximately 1000 mm. As the capital of Anhui Province, it is considered to be the economic, educational, and transportation center of central China, and is one of China's three major science centers. Since China's "Open and Reform Policy" started in 1978, the area has shown striking signs of urban expansion. In the past 30 years, due to the rapid socioeconomic development and urbanization process, the land use structure and ecological service functions of Hefei have been altered, which have had a certain impact on the stability of the ecosystem. After 2011, the administrative boundaries in Hefei were changed. This study uses a range of administrative areas before the change occurred as the research area.

Data description and preprocessing

We first collected the available summer Landsat-5, Landsat-7, and Landsat-8 images from 1987 to 2017. Due to the effects of clouds, the Landsat/ETM+ SLC-off problem, and other image-specific problems, much of the data needed for this study were missing in the study area. Therefore, satisfactory summer Landsat images were only available for a total of 6 years (1987, 1992, 1997, 2002, 2007, and 2017). These images were selected, based on their phenology and scene quality (i.e., minimum cloud cover standards, better vegetation coverage, and optimal time periods for discriminating land cover types). In order to obtain continuous summer Landsat-like data with 30-m spatial resolution, some Landsat (out of the date range) and MOD09A1 data were collected for STF. In order to fit with the Landsat data, MOD09A1 data were re-projected to the Universal

Transverse Mercator (UTM) projection system (Datum WGS84 and Zone 50) using the MODIS re-projection tool, and were resampled to a spatial resolution of 30 m, using the cubic interpolation approach. Preprocessing tasks such as radiation calibration, FLAASH atmospheric corrections, image mosaicking, and image cropping were applied before classifying the images using the ENVI tool.

Method

Spatiotemporal data fusion

The STF method was employed to offset the trade-off between the temporal and spatial resolutions of the different sensors, and to obtain high spatiotemporal resolution data (Gao et al. 2006). In consideration of the fact that the landscapes of Hefei City are very heterogeneous, the enhanced spatiotemporal adaptive reflectance fusion model (ESTARFM) was adopted as a priority in this study (Emelyanova et al. 2013). The two pairs of MODIS and Landsat images (date of t_m and t_n) and one MODIS image at the prediction date t_p can be used as the reference to compute the Landsat-scale image of the prediction date t_p , and to mark the results as $F_m(x_{w/2}, y_{w/2}, t_p, B)$ or $F_n(x_{w/2}, y_{w/2}, t_p, B)$, respectively. A more accurate reflectance at t_p can be obtained by a weighted combination of the two prediction results (Zhu et al. 2010). The predicted Landsat-scale reflectance at t_p can be calculated as

$$F(x_{w/2}, y_{w/2}, t_p, B) = T_m \times F_m(x_{w/2}, y_{w/2}, t_p, B) + T_n \times F_n(x_{w/2}, y_{w/2}, t_p, B) \quad (1)$$

where (x, y) is the location of a given pixel; w is the width of the searching window, where similar pixels are selected for calculating the reflectance value of the central pixel ($X_{w/2}, Y_{w/2}$). The size of the window is determined by the heterogeneity of the study area, which grows larger as the heterogeneity of the study area increases; B indicates the band, and T_m and T_n indicate the temporal weights, which are calculated based on the magnitude change detected by the resampled coarse-resolution reflectance between time $t_{m/n}$ and the prediction time t_p . In the ESTARFM algorithm, two pairs of fine-resolution and coarse-resolution images at times t_m and t_n are used. Either pair of the reflectance image at t_m

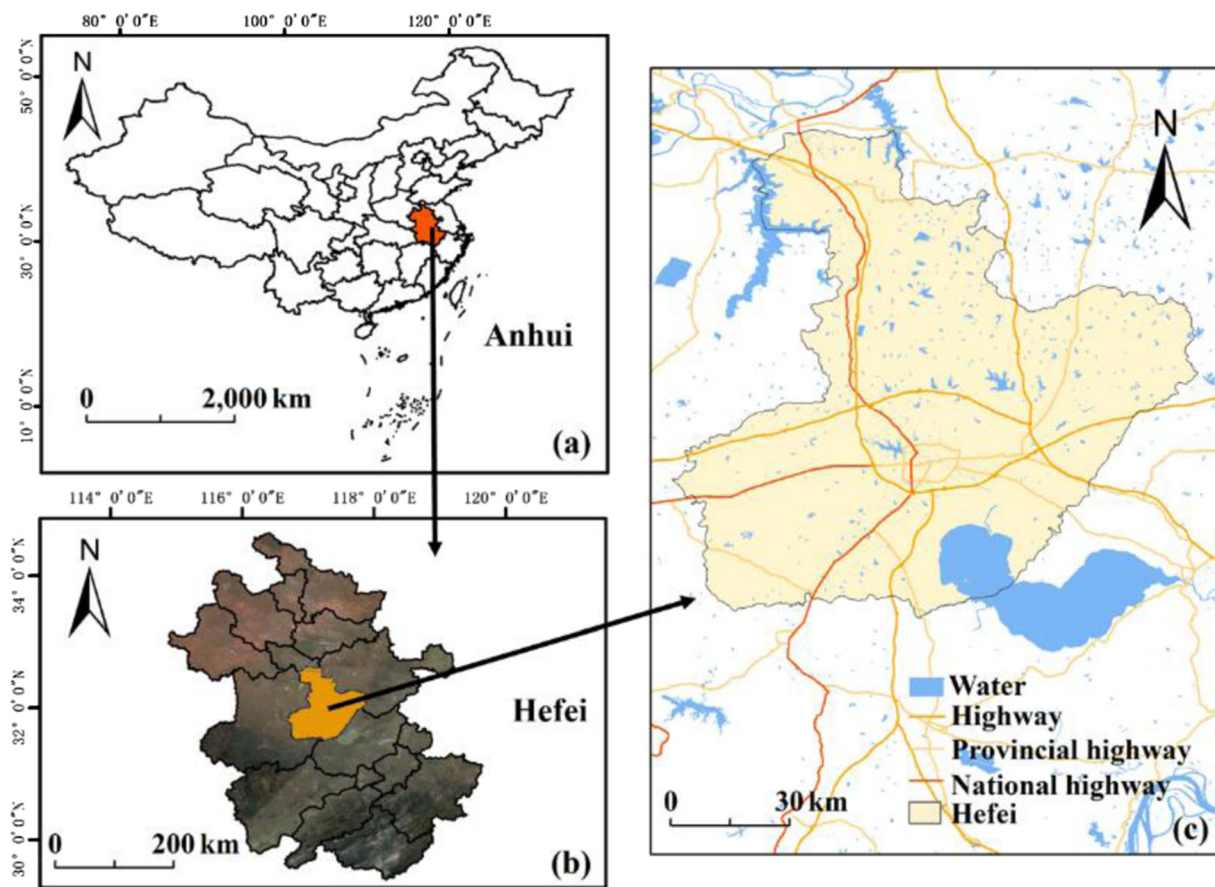


Fig. 1 Location map of the study area. (a) The location of Anhui province in China. (b) The administrative boundary of Hefei in Anhui province. (c) The map of the study area

and t_n can be used as the base date to compute the fine-resolution reflectance of the prediction date t_p . A more accurate reflectance at t_p can be obtained by a temporal weighted combination of the two prediction results. A detailed description of the ESTARFM algorithm can be referred to in Zhu et al. (2010).

Land cover classification and accuracy assessment

Image classifications were carried out to extract useful thematic information from the nine Landsat images in Table 1. Image classification uses a hybrid classification technique that combines unsupervised and supervised classification techniques (support vector machines, SVMs). The SVM with a radial basis function in ENVI 5.3 software was used for LULC classification. Some parameters such as gamma in the kernel function, penalty parameter, pyramid levels, and classification probability threshold were set according to the default

values. The hybrid classification technology can improve the classification accuracy better than a single classification method alone (Gashaw et al. 2017). According to the “Classification of Land Use Status”, jointly promulgated by the General Administration of Quality Supervision, Inspection, Quarantine and Standardization Administration of the People’s Republic of China, in combination with the status and characteristics of land use in the study area, the land use types were divided into four categories: cultivated land (dry land and paddy fields), construction land (residential areas, industrial land, and transportation land), water (rivers, reservoirs, lakes, and ponds), and vegetation (grass, shrubs, and trees).

To perform the accuracy assessment for the classified images, 538 uniformly distributed points were generated across each LULC map (shown in Fig. 2). These points were then crosschecked with the reference data. The classified images were compared with the reference

Table 1 Accuracy assessment results of historical land use and land cover classification

	1987	1992	1997	2002	2007	2011	2012	2014	2017
Overall accuracy (%)	95.17	94.61	93.87	93.68	92.94	90.52	92.19	94.57	93.87
Kappa coefficient	0.89	0.88	0.84	0.88	0.87	0.82	0.86	0.90	0.88

images through the error matrix (Ariti et al. 2015). The overall accuracy and Kappa coefficients are shown for the accuracy assessment. In this study, it is very difficult to obtain the LULC reference data for the classification accuracy, due to the long LULC change analysis sequence. Therefore, remote sensing images (such as Landsat and GF-1/2 satellites) and Google Earth images were taken as reference data for the accuracy assessment from corresponding time periods. If the high-resolution images could be obtained (such as GF-1/2 images or Google Earth images), the random sample points were classified through visual interpretation, using high-resolution images as the reference images. Otherwise, visual interpretation was done by using the Landsat images as the reference images. Taking the year 2002

as an example, Fig. 2 shows the locations of the 538 sample points for the accuracy detection of the classified images. The accuracy reports for the classified images in 1987, 1992, 1997, 2002, 2007, 2011, 2012, 2014, and 2017 are presented in Table 1. The overall accuracy is higher than 90%, and the Kappa coefficients are higher than 0.82, which meet the requirements of this study.

Land use and land cover prediction

The prediction of the LULC information for this study was undertaken with the cellular automata–Markov (CA–Markov) model, which combines the advantages of the Markov chain in predicting long time series, and CA, based on spatial relationships, and it can more

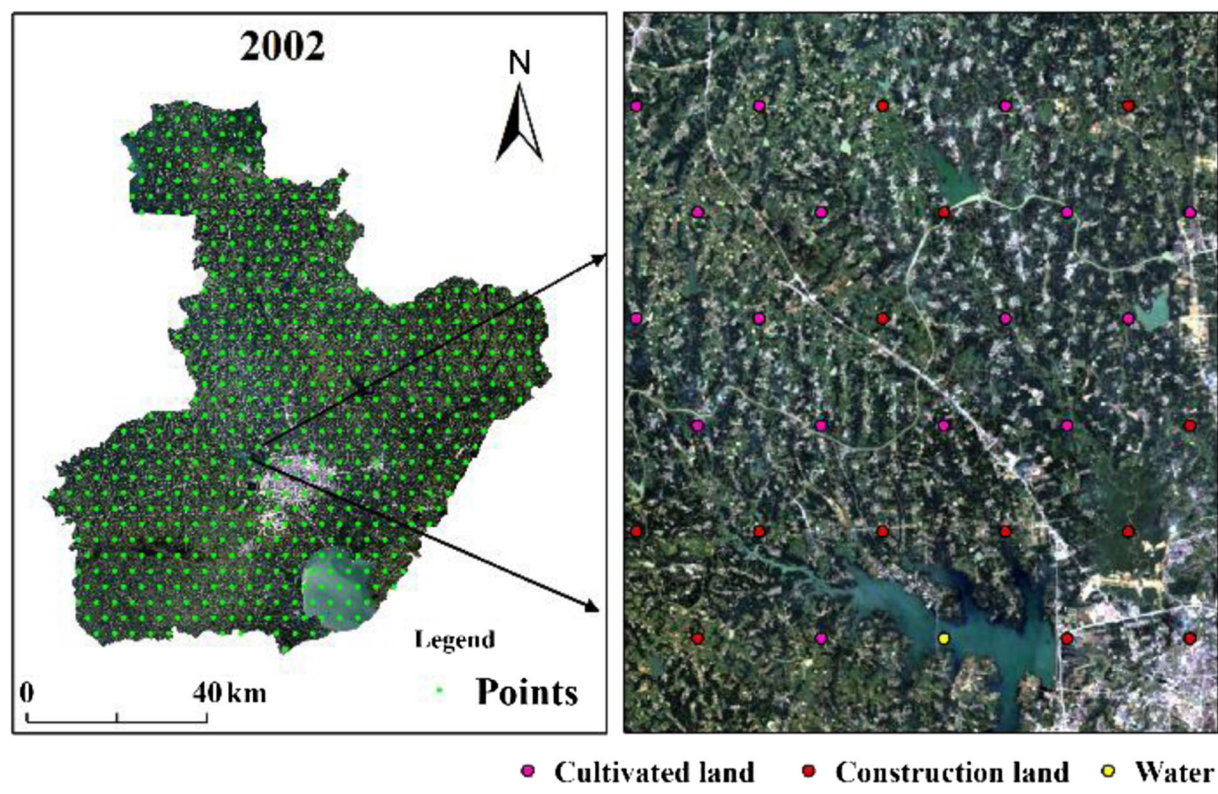


Fig. 2 Location of 538 uniformly distributed sample points

accurately simulate LULC changes in time and space (Fu et al. 2018). In theory, when using the CA–Markov model for a prediction, the simulated period is equal to the inter-annual interval between the base and the end images used for the prediction (Wang et al. 2018).

The Markov model is a stochastic model that is mainly used for LULC modeling. In the Markov process, the state of the system is related only to the current state. The Markov model describes the land use change from one period to another, based upon which it predicts the future trends in the LULC change (Muller and Middleton 1994). The following formula can be used to predict the LULC:

$$S_{t+i} = P_{ij}S_t \quad (2)$$

where S_t and S_{t+1} are the states of the land use structure at t and $t+1$, respectively, and P_{ij} is the state transition matrix.

Cellular automata represent a type of grid-dynamic model with strong space-computing power. The time, space, and state of the model are discrete. The spatial interactions and time causality are local, and the model has the ability to simulate the spatiotemporal evolution of complex systems (Blecic et al. 2013; Liu et al. 2017a, b). The CA model can be expressed as follows:

$$S_{t+i} = f(S_t, N) \quad (3)$$

where S is a finite, discrete states set of cells; N is the cellular neighborhood; t and $t+i$ are different moments; and f is the cell transformation rule of the local space.

The detailed parameters and steps of the LULC prediction, using the CA–Markov model, are as follows: (1) Data format conversion and reclassification are performed to obtain fixed land use types. (2) Using the Markov module, the state transition probability matrix and the transfer area matrix are obtained. (3) A transition suitability image set is established. In this paper, we used the conditional probability image output by the Markov model as a transition suitability image set, to better maintain the transfer trend between the base period and the last period, and removed the artificial interference generated when calculating the relative weight factor. (4) The CA filter and the number of cycles are determined; in this paper, a 5×5 filter was used; that is, the matrix space composed of 5×5 cells around each central cell had a significant effect on the change in the cellular state. (5) An error matrix is used to assess the accuracies of the prediction images according to the

actual images. Some commonly used statistical indices, such as the user accuracy, producer accuracy, overall accuracy, and Kappa coefficient, are reported for the accuracy assessment. The number of cycles is equal to the inter-annual interval between the base and end images used for the prediction (Derya 2015; Palmate et al. 2017).

This study uses the CA–Markov model for the prediction of LULC. There are two main reasons: First, although the CA–Markov model has a weak ability to capture new random development areas because some factors, such as socioeconomic, policy, and demographic data are not considered, a large number of scholars have still used the model for urban LULC prediction (Derya 2015; Kityuttachai et al. 2013; Guan et al. 2011; Jafari 2016). Second, the high prediction accuracy of LULC from the CA–Markov model can be obtained if the input maps are in short inter-annual intervals. Actually, the purpose of this paper is to use spatiotemporal data fusion to obtain high temporal frequency LULC maps, shorten the year interval of prediction, and improve the prediction accuracy of the CA–Markov model. Therefore, combining the spatiotemporal data fusion and CA–Markov model can improve the prediction accuracy of LULC.

Figure 3 shows a detailed flowchart of the methodology used in this study. In the presence of summer Landsat images, we extracted the LULC information directly after the image preprocessing step. In the presence of non-summer Landsat images, spatiotemporal data fusion was employed to predict the desired Landsat data, by using a MODIS image of the ideal range, two Landsat images out of the ideal range, and the auxiliary of the corresponding MODIS, after which we extracted the LULC information. The obtained data were used to predict the LULC and to evaluate the accuracy. Table 2 shows the processing methods for the LULC information of the different years.

Results and analysis

In this section, validation experiments of the fusion methods were firstly conducted, where the simulated Landsat-like images at the required time were generated. Then, many experiments were performed to explore whether the simulated LULC maps from the STF method were feasible for LULC prediction. After confirming the feasibility of the STF method in the LULC

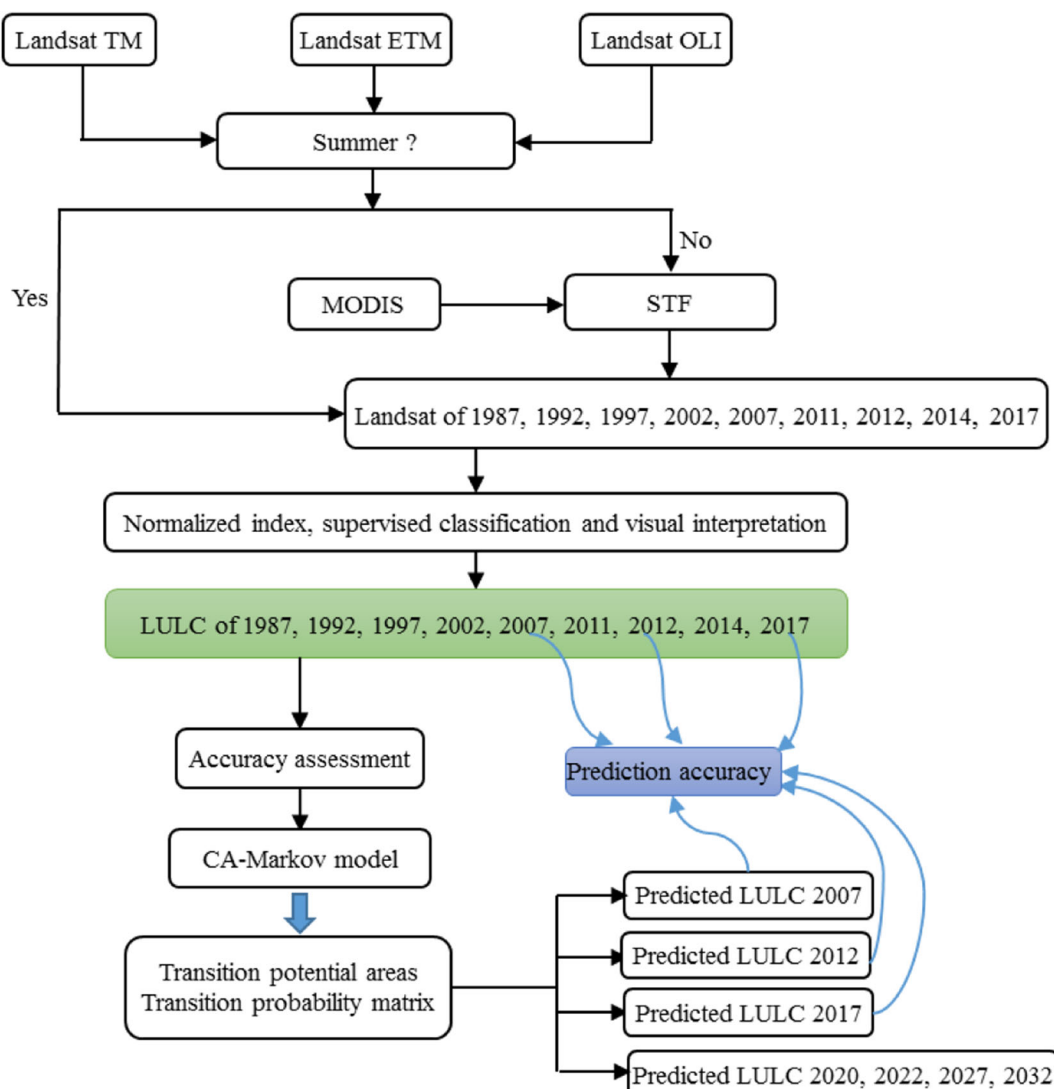


Fig. 3 Flowchart of the methodology used in the present study

prediction, predictions from different inter-annual intervals were compared. Fourth, quinquennial summer Landsat-scale images were obtained, to analyze the LULC change information from 1987 to 2017. Finally, LULC maps of 2020, 2022, 2027, and 2032 were predicted.

Simulated validation of the fusion methods

The accuracy of the STF method depends not only on the fusion model used, but also on the characteristics of the input image pairs. The ESTARFM needs to be modified when: (1) only one pair of Landsat and MODIS images can be obtained in the same year; (2)

one of the two pairs of Landsat and MODIS images decrease the precision, because of the inconsistency between the coarse- and fine-resolution images, the time lag between the pairs and prediction dates, and so on (Xie et al. 2018). In these cases, the one pair of Landsat and MODIS images should be used for both t_m and t_n when ESTARFM was implemented, and also to obtain better predictions.

Considering the actual situation, in addition to the fused result from two different pairs of Landsat and MODIS images at t_m and t_n , the other two fused results are obtained from two pairs of Landsat and MODIS images are the same data, such as at t_m or t_n . The best fused result was selected for this study. As an example,

Table 2 Processing methods for the LULC information of the different years in Hefei. Note that the MODIS data were acquired as 8-day composites; to fit with the Landsat data, the dates given in the table are the corresponding days of the 8-day acquisition period, respectively

Year	Method	TM/ETM+/OLI	MODIS	LULC
1987	Extraction of LULC	1987.08.11		1987.08.11
1992	Extraction of LULC	1992.07.23		1992.07.23
1997	Extraction of LULC	1997.06.03		1997.06.03
2002	Extraction of LULC	2002.08.04		2002.08.04
		2007.05.06	2007.05.06	
2007	Extraction of LULC	2007.08.02	2007.08.02	2007.08.02
	(Extraction of LULC after STF)	2007.10.05	2007.10.05	
		2011.04.23	2011.04.23	
2011	Extraction of LULC after STF		2011.07.11	2011.07.11
		2011.10.08	2011.10.08	
		2012.04.01	2012.04.01	
2012	Extraction of LULC after STF		2012.07.27	2012.07.27
		2012.11.11	2012.11.11	
		2014.05.01	2014.05.01	
2014	Extraction of LULC after STF		2014.08.14	2014.08.14
		2014.10.24	2014.10.24	
2017	Extraction of LULC	2017.06.02		2017.06.02

prediction from two pairs of Landsat and MODIS images acquired on 6 May 2007 and 5 October 2007 and another MODIS images at the predicted time (2 August 2007) was named RESULT_A. Predictions from MODIS images acquired on 2 August 2007, and one pair of Landsat and MODIS images acquired on 6 May 2007 or 5 October 2007 were named RESULT_B and RESULT_C, respectively. Scatter plots in Fig. 4 show the relationship of the reflectance between the fused results (RESULT_A, RESULT_B, and RESULT_C), and the actual Landsat data acquired on 2 August 2007, for the green, red, NIR (Near Infrared), and SWIR (short-wave infrared) bands, respectively. The data in the scatter plots fell close to the 1:1 line, indicating that the STF method can capture the reflectance changes. For a quantitative evaluation of the results, the average absolute difference (AAD) and the coefficients of determination (R^2) of the simulated reflectance, compared to actual reflectance, were calculated. From Fig. 4, overall, we can see that the scores from RESULT_B ($AAD = 0.0252, 0.0268, 0.0510, 0.0304; R^2 = 0.7014, 0.6859, 0.7718, 0.7705$) were better than those from RESULT_A ($AAD = 0.0271, 0.0270, 0.0814, 0.0265; R^2 = 0.5652, 0.5817, 0.6625, 0.8036$) and RESULT_C ($AAD = 0.0266, 0.0257, 0.0448, 0.0314; R^2 = 0.6324, 0.6161, 0.7905, 0.7506$).

Figure 5 shows the MODIS images acquired on 2 August 2007, one pair of Landsat and MODIS images acquired on 6 May 2007, RESULT_B, and the actual Landsat image acquired on 2 August 2007. From the perspective of visual analysis, we could see that obvious phenological and seasonal rhythm changes had occurred between the Landsat acquired on 6 May 2007 and 2 August 2007. The fused result (RESULT_B) was very close to the actual Landsat image acquired on 2 August 2007, which indicates that the STF method successfully captured these change information from MODIS observations to estimate the Landsat reflectance. To enhance visual judgment, two detailed regions cropped from Fig. 5(d)–(e) are shown in Fig. 5. It is clear that the locations of cultivated land, construction land, water, and vegetation in the fusion image were almost the same as that of the actual image, and the characteristics and areas of the land use types were also very close. Although the fused result was slightly more blurred than the actual image, and also produced some errors, the fused images were still quite similar to the actual images than images acquired from different seasons. The above experiments show that the STF method is feasible and applicable for the generation of Landsat-like images at the required time. Therefore, according to the same method, simulated images for 11 July 2011, 27 July 2012, and 14 August 2014 could also be obtained.

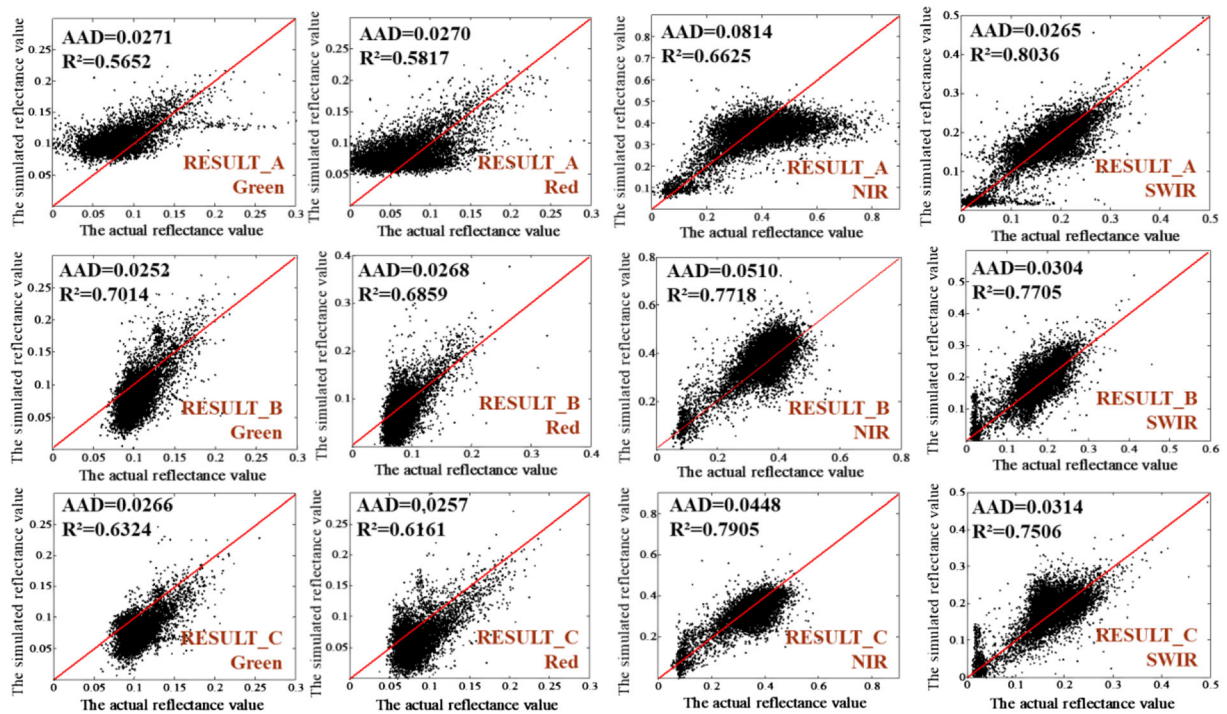


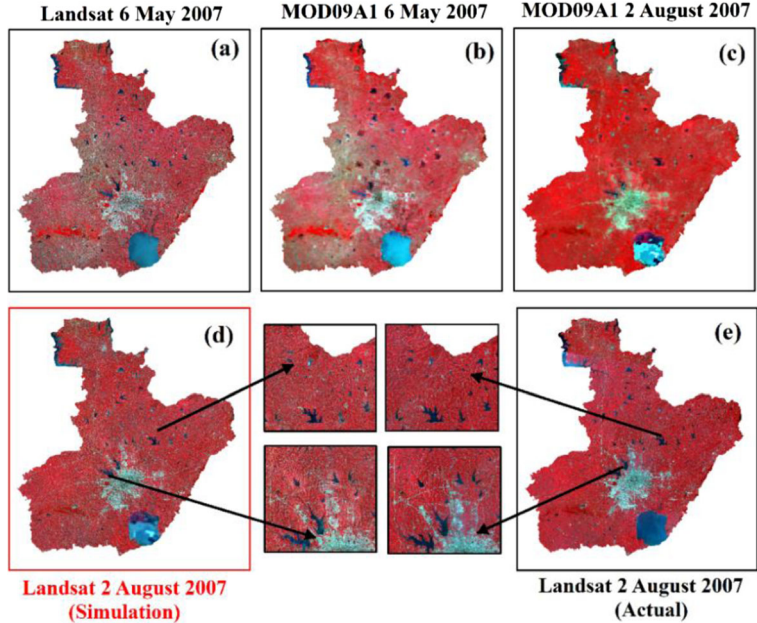
Fig. 4 Scatter plots of the actual reflectance and the simulated reflectance from ESTARFM with different input image pairs for the green, red, NIR, and SWIR bands, respectively

Prediction of LULC accuracy based on the STF method

In this section, two experiments (EXP1 and EXP2) were conducted to explore whether the STF method is feasible in LULC prediction (shown in Fig. 6). For EXP1,

the CA–Markov model was used to predict the 2017 LULC data, based on the actual summer Landsat LULC data of 1997 and 2007. For simplicity, this description is termed 1997(A)+2007(A). Then, the actual Landsat 2007 LULC data were replaced with the fused LULC

Fig. 5 Simulated validation of the STF method (the order of the band: NIR, red, green). (a) Actual Landsat image acquired on 6 May 2007; (b) actual MODIS image acquired on 6 May 2007; (c) actual MODIS image acquired on 2 August 2007; (d) simulated Landsat-like image acquired on 2 August 2007 by the STF method; (e) actual Landsat image acquired on 2 August 2007



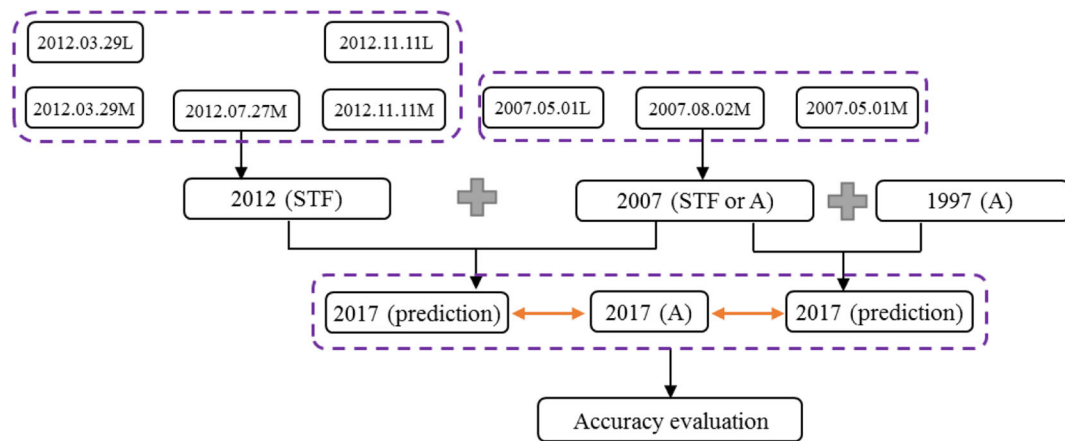


Fig. 6 Experimental flowchart of the feasibility of the STF method for the LULC prediction (A: the actual LULC data, STF: the fused LULC data, L: the Landsat data)

data of 2007, which were generated by fusing the Landsat and MODIS images at the base date, and the MODIS image at the predicted date (2 August 2007) (1997(A)+2007(STF)). The actual 2017 LULC data were used to assess the prediction results. For EXP2, the actual LULC data of 2007 and the fused LULC data of 2012 (the fused LULC data of 2012 were generated based on the Landsat and MODIS images at the base date, and the MODIS image at the predicted date (27 July 2012)) were used to predict the LULC data of 2017 (2007(A)+2012(STF)). Then, the actual 2007 LULC data were replaced with the fused LULC data of 2007 again (2007(STF)+2012(STF)), and the prediction result was compared with the actual 2017 LULC data. The actual LULC map of 2017 and the results of the prediction using actual images and fused images are shown in Fig. 7, and the two partial enlargements show more details of the prediction results. By visual comparison, the prediction results based on the fused remote sensing images and actual images were reasonably similar (Fig. 7(a) and (c); (b) and (d)), and the spatial structure of the prediction results were very close to the actual LULC of 2017. The magnified view of the two selected areas also showed that all land use types had a high degree of spatial consistency.

To further validate the feasibility of the STF method in LULC prediction, we performed quantitative analysis on two sets of experiments. Each of the four predicted maps (EXP1 and EXP2) were overlapped with the actual maps in 2017, and the confusion matrices were employed to calculate the overall accuracy and the Kappa coefficients (Table 3). Table 3 shows the accuracy of the prediction results, and the overall accuracy was

higher than 84%, and the Kappa coefficient was higher than 0.71. According to Monseru (1992) (Monseru and Leemansb 1992), a Kappa coefficient of between 0.70 and 0.85 was generally rated as being a very good indicator of the classified image in representing the actual image. The results indicate that the CA–Markov model successfully predicted LULC in this study, and that the model can also be reliably used for the prediction of future land use changes in the area. The overall accuracy of the prediction results based on the fused data were 84.84% and 87.11%, and the Kappa coefficients were 0.7128 and 0.7601, respectively. High Kappa coefficients and overall accuracies indicate that the fused data are feasible for LULC prediction. The overall accuracy of the prediction results based on the actual data were 85.10% and 87.76%, and the Kappa coefficients were 0.7185 and 0.7697, respectively. Highly similar values of the Kappa coefficients and overall accuracy indicated a general consistency between the prediction results of the fused data and actual data. Figure 8 shows that the areal extents of the two types of prediction results also illustrate the acceptable range of decisions, in which the predicted areas of cultivated land were 59.86% and 58.38% in the actual maps, while the predicted areas of cultivated land were 60.24% and 57.54% in the fused maps, respectively. There were approximately equal proportions of construction land in the two types of prediction. In addition, the proportions of water and vegetation in the prediction results were also approximately equal when using the actual data and the fused data. These results show that the data obtained by STF are suitable for LULC prediction, and that they have high usability and validity.

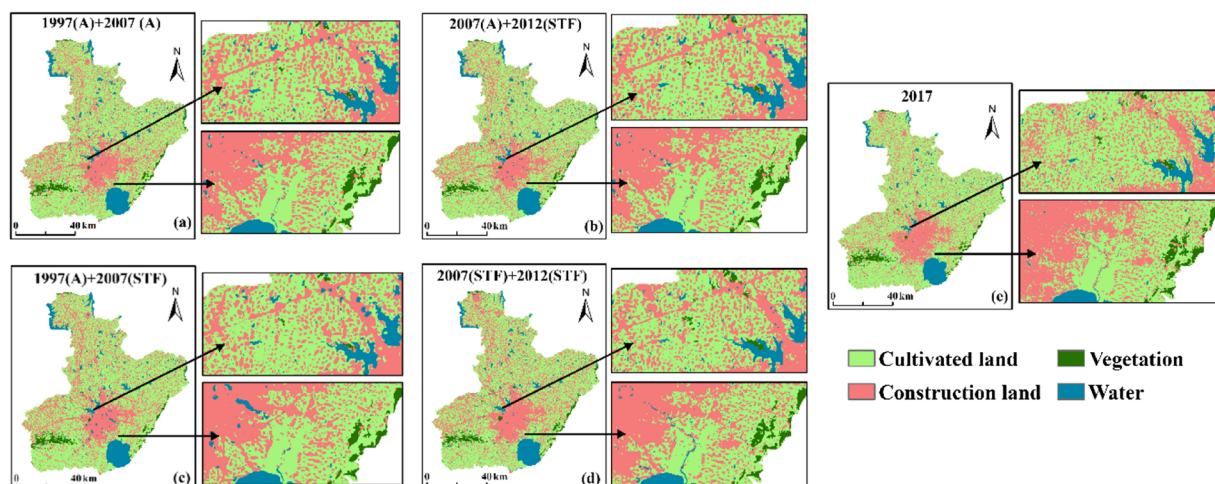


Fig. 7 Comparison of predicted LULC by using the actual and fused LULC map in 2017, respectively. (a) Predicted LULC for 2017 based on the actual LULC map of 1997, 2007; (b) predicted LULC for 2017 based on the actual LULC map of 2007 and the

fused LULC map of 2012; (c) predicted LULC for 2017 based on the actual LULC map of 1997 and the fused LULC map of 2007; (d) predicted LULC for 2017 based on the fused LULC map of 2007, 2012; (e) the actual LULC of 2017

The user accuracy and producer accuracy of each land use and land cover type derived from the LULC prediction images for the four prediction images are shown in Table 4. The user accuracies of all land use and land cover types were higher than 80%, and the producer accuracy of all land use and land cover types were higher than 73%. The user accuracy and producer accuracy of each land use and land cover type in the prediction results of the fused data were close to the prediction results of the actual data. The relatively low prediction accuracy of construction land was due to the acceleration of the urbanization process, and the increase of man-made disturbances in the construction land, which has led to significant changes in the LULC in the short term. However, this CA–Markov model has a weak ability to capture new random development areas (Singh et al. 2015; Mosammam et al. 2016). We conclude that the STF method can acquire high temporal frequency, same-season LULC maps, and predict the LULC for a particular year, which can show more detailed trajectories of land use changes and feedback loops, and provide scientific references for policy makers in urban management and further planning.

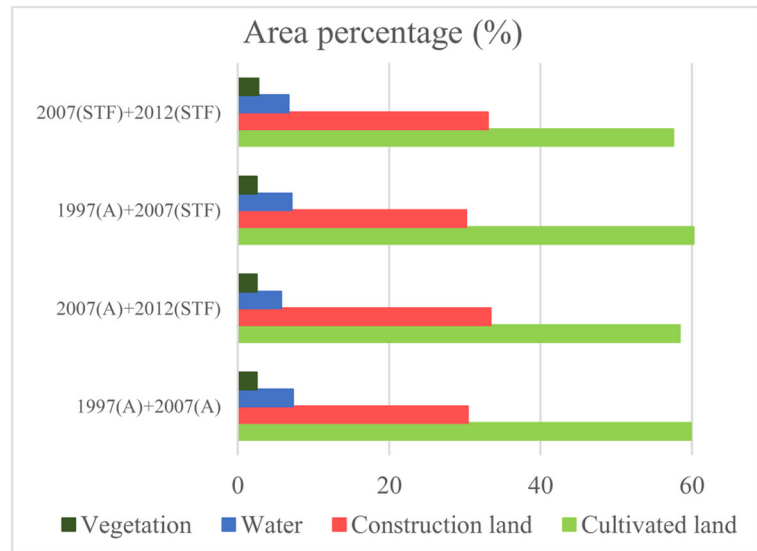
Comparison of LULC prediction accuracy under different inter-annual intervals

After confirming the feasibility of the STF method in the LULC prediction, we obtained high temporal frequency, same-season LULC maps to compare the prediction accuracy of different inter-annual intervals. The LULC maps of 1987, 1997, 2002, 2007, 2011, 2012, and 2014 were used to predict the 2017 LULC. These LULC data were divided into four groups, namely, 1987+2002, 1997+2007, 2007+2012, and 2011+2014, with inter-annual intervals of 15, 10, 5, and 3 years, respectively. Note that the LULC data of 2014 were fused by using the Landsat and MODIS images at the base date, and the MODIS image at the predicted date (14 August 2014). The predicted LULC maps from different inter-annual intervals and the actual LULC of 2017 are shown in Fig. 9. Visually, with a decline in the inter-annual interval, the spatial distribution characteristics of each land use and land cover type in the predicted LULC of 2017 were more similar to the actual LULC of 2017 (Fig. 9). Furthermore, Fig. 10 shows the quantitative results of the LULC prediction with different inter-annual

Table 3 Accuracy assessment of the predicted LULC by using the actual and fused LULC maps, respectively

	1997(A)+ 2007(A)	1997(A)+ 2007(STF)	2007(A)+ 2012(STF)	2007(STF)+ 2012(STF)
Overall accuracy (%)	85.10	84.84	87.76	87.11
Kappa coefficient	0.7185	0.7128	0.7697	0.7601

Fig. 8 Graphical representation of the predicted LULC by using the actual and fused LULC maps, respectively



intervals. The overall accuracy of the prediction results derived from the inter-annual intervals of 3, 5, 10, and 15 years were 90.48%, 87.76%, 85.10%, and 82.36%, respectively, and the Kappa coefficients were 0.8200, 0.7697, 0.7185, and 0.6578, respectively. The user accuracy and producer accuracy of each land use and land cover type were derived from the LULC prediction images for the four prediction images in Table 5. The producer accuracy of cultivated land was higher than 86%, and the user accuracy of cultivated land was higher than 85%. The producer accuracy of construction land was higher than 70%, and the user accuracy of the construction land was higher than 72%. The results show that the prediction accuracy was high, and that it met the requirements of this study. The table shows that with the shortening of inter-annual intervals, the user accuracy and producer accuracy continued to increase.

When the inter-annual interval was 3 years, the producer accuracy and user accuracy of the cultivated land were 95.83% and 87.67%, respectively, and the producer accuracy and user accuracy of the construction land were 78.45% and 92.96%, respectively. So, as a conclusion, we can see that shorter inter-annual intervals in the prediction process led to a higher prediction accuracy of the LULC. It can be concluded that the STF method can shorten the predicted inter-annual interval, to improve the LULC prediction accuracy, and provide a reliable basis for future land use planning and ecological environment protection.

Detection of quinquennial LULC over the last 30 years

Based on the STF method, quinquennial summer Landsat-scale images were obtained, to analyze the

Table 4 Accuracy assessment of each land use and land cover type for the prediction result by using the actual and fused LULC maps, respectively

	Cultivated land	Construction land	Water	Vegetation
Producer accuracy (%)				
1997(A)+2007(A)	91.00	73.17	77.98	94.11
1997(A)+2007(STF)	91.08	73.18	78.07	94.31
2007(A)+2012(STF)	94.42	74.29	94.94	95.71
2007(STF)+2012(STF)	94.71	74.01	85.74	88.93
User accuracy (%)				
1997(A)+2007(A)	85.91	80.35	91.74	87.56
1997(A)+2007(STF)	85.97	80.35	91.84	88.35
2007(A)+2012(STF)	86.38	90.27	90.29	89.25
2007(STF)+2012(STF)	85.41	89.06	95.17	89.67

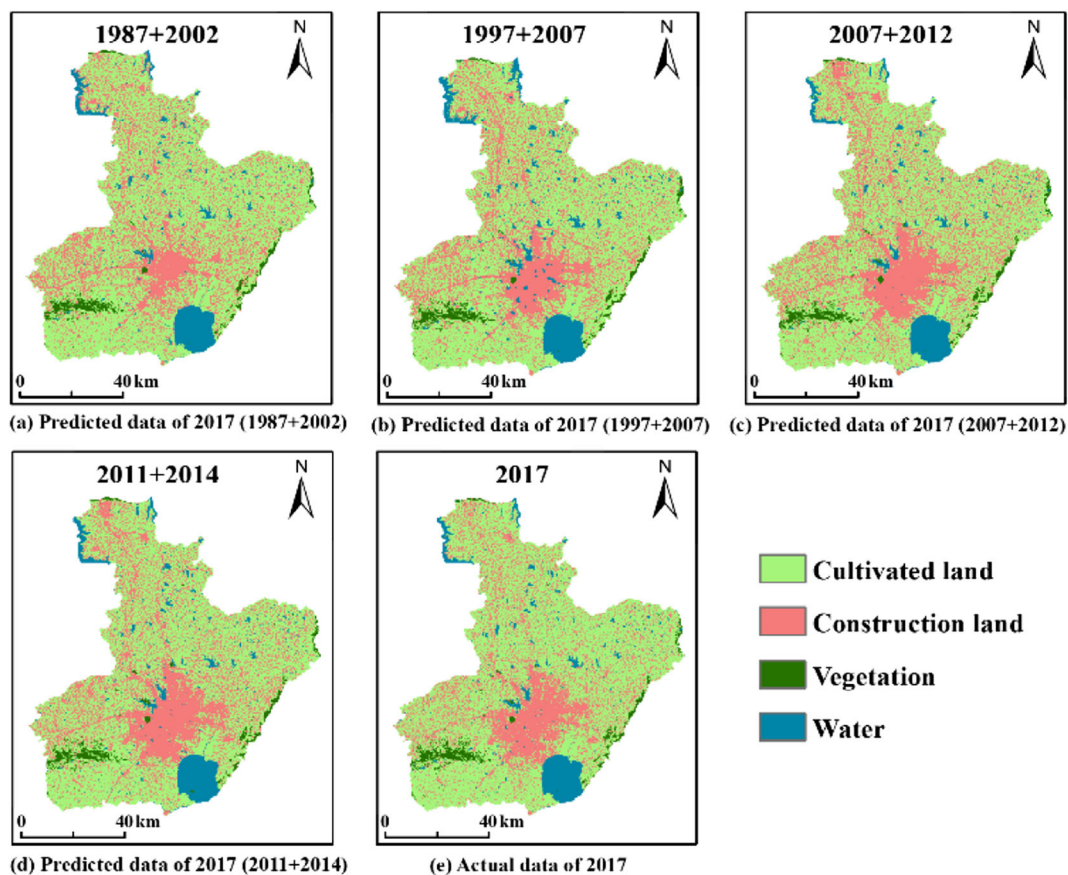


Fig. 9 The predicted LULC maps under different inter-annual intervals

LULC information. Since 1987, there are seven LULC maps: 1987, 1992, 1997, 2002, 2007, 2012, and 2017. From a time perspective, from 1987 onward, among the dominant landscapes in Hefei, the area of cultivated land declined from 77.83 to 63.82% over the last 30 years

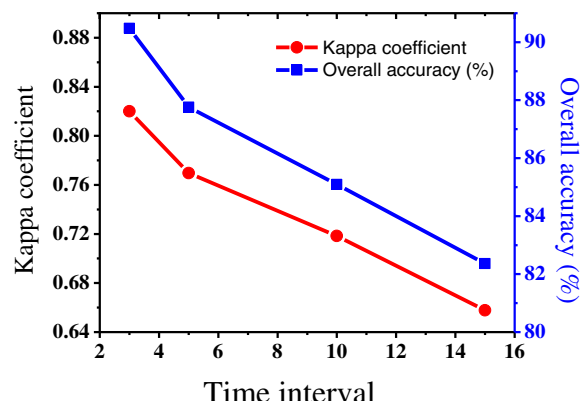


Fig. 10 Accuracy assessment of the prediction results under different inter-annual intervals

(Fig. 11). Meanwhile, the area of construction land increased from 13.17% to 27.47%. The natural landscape changed quickly to an artificial landscape, due to the rapid development of urbanization in Hefei. A steady population increase occurred as a result of external migration and rural depopulation because of job opportunities and a better quality of life, which increased the demand for housing, and thus increased the construction land. The areas of water and vegetation showed an overall downward trend; however, they were in a relatively stable state (the area of water declined from 6.12 to 6.03%, while that of vegetation declined from 2.88 to 2.68%) due to the ecological civilization construction in Hefei, and the strengthening of the protection of green spaces and water resources.

From a spatial perspective, it can be seen that the spatial distributions of all land use types did not change significantly from 1987 to 1997 (Fig. 12). After 1997, the rate of change continued to increase, and the most direct change was the significant expansion of

Table 5 Accuracy assessment of each land use and land cover type of prediction result, in inter-annual intervals

	Cultivated land	Construction land	Water	Vegetation
Producer accuracy (%)				
1987+2002	86.93	70.04	88.11	94.47
1997+2007	91.36	73.38	79.32	94.32
2007+2012	94.04	77.06	91.08	94.42
2011+2014	95.83	78.45	83.99	86.91
User accuracy (%)				
1987+2002	85.77	72.71	89.97	82.96
1997+2007	85.70	81.20	95.68	86.86
2007+2012	88.08	88.56	92.55	88.90
2011+2014	87.67	92.96	89.89	84.78

construction land in the form of the occupation of cultivated land. Most of the increase in construction land occurred in the center of this city. From 1987 to 2007, the construction land mainly expanded southwestward. As one of the four science and education bases in China, Hefei has established a cultural and educational gathering area in the southwest, to speed up urbanization in Southwest China. After 2007, the expansion in the south was larger, mainly because the Binhu New Area in Hefei represents a pioneer of the development strategy of “a great city of lakes, also known as an innovation-oriented high ground” in Hefei. The rapid development of the tertiary industry, led by finance, tourism, culture, commerce, trade, and information technology, accelerated the urbanization of the southern urban areas. Figure 12 shows that the central urban district of Hefei and “multi-satellite towns” did not develop simultaneously. In contrast, the central urban district merged with the sub-central urban district to form a larger central city area.

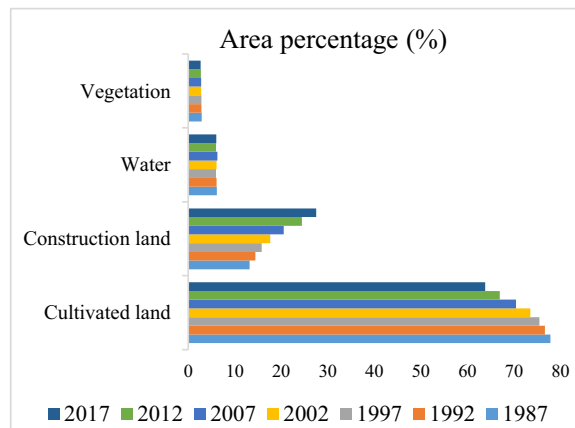


Fig. 11 Graphical representation of historical land use and land cover

Hefei, as the political, economic, and cultural center of Anhui Province, has experienced rapid economic developments over the past 30 years. As a result, the population has increased significantly, and the downtown area has been overexpanded, which increases the vulnerability of the ecological environment to some extent. For future urban development, the government should take various measures to effectively solve problems, such as the loss of arable land, the shortage of water resources, and the overexploitation of forests, and it should aim to achieve sustainable development in Hefei.

LULC prediction

In this study, satellite-derived LULC maps of 2002, 2007, 2012, 2014, and 2017 were used to predict the LULC maps of 2020, 2022, 2027, and 2032 in Fig. 13 (2014+2017, 2012+2017, 2007+2017, and 2002+2017, respectively). Figure 14 shows the area of future land use and land cover types from 2007 to 2032. The results show an increase in the area of construction land from 20.53 to 39.56%, and a decrease in the area of cultivated land from 70.41 to 52.04%, while the areas of water and vegetation changed from 6.27 to 5.99%, and from 2.79 to 2.41%, respectively, during the years of 2007–2032, as shown in Fig. 14. Figure 15 shows that the area of cultivated land decreased by 11.47%, 3.89%, and 4.18%, respectively, and the area of construction land increased by 26.25%, 9.21%, and 4.45, respectively, during the years 2017–2022, 2022–2027, and 2027–2032. The increase in construction land and the decrease in cultivated land peaked during 2017–2022, and then the rate of change eased. To explore the future processes of urbanization in detail, and to generate timely

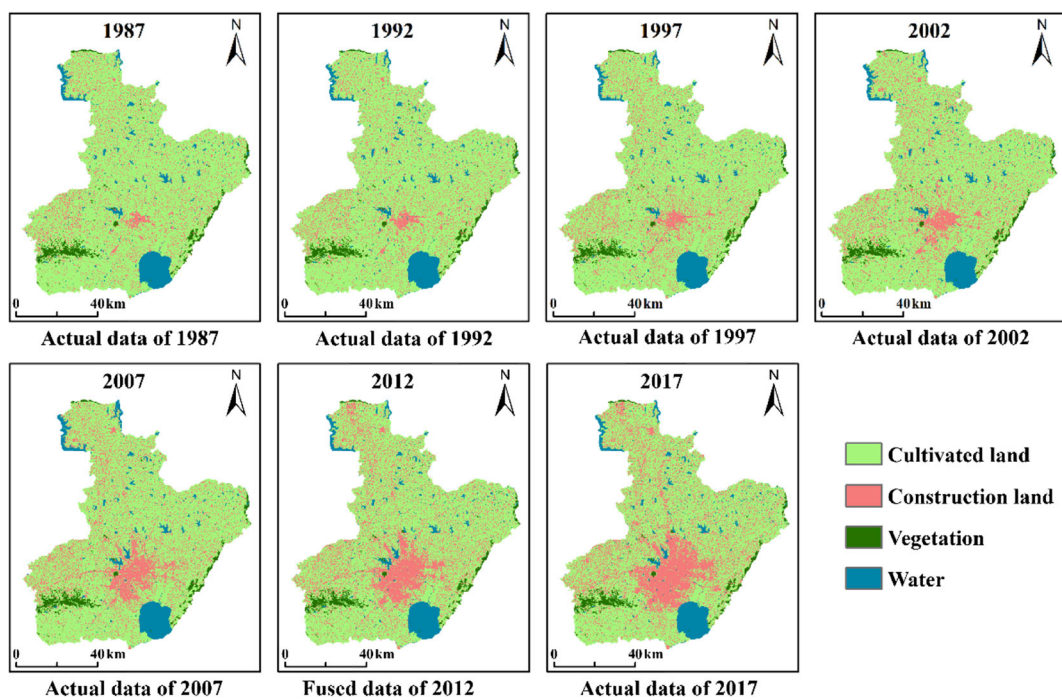


Fig. 12 Satellite-derived historical land use and land cover classification maps

countermeasures, we used the STF method to obtain LULC prediction data for a particular year, to further refine future LULC change estimations. As seen from Fig. 15, the average annual increase in construction land and the average annual decrease in cultivated land

peaked during 2017–2020; the increase in the area of construction land was 3.18%, and the decrease in the area of cultivated land was 8.00% on average each year. The rate of urban expansion peaked during 2017–2020. The main factors driving the change of LULC were the

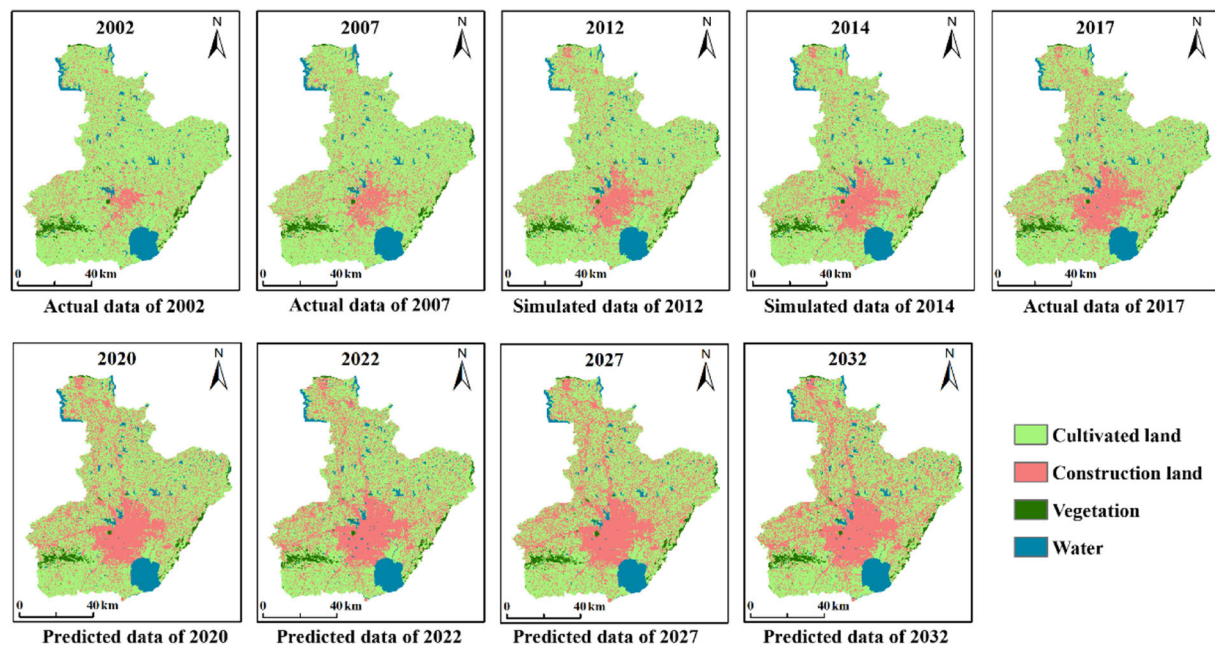


Fig. 13 Land use and land cover maps for 2007, 2012, 2017, 2020, 2022, 2027, and 2032



Fig. 14 Graphical representation of land use and land cover for 2007, 2012, 2017, 2020, 2022, 2027, and 2032

mutual restraint between land urbanization and ecological environment protection. Urgent measures must be taken to constrain the intensity and speed of urbanization, in order to slow down soil erosion, vegetation damage, and land degradation. It is a major challenge to reconcile land use and to protect the urban ecological environment over the next 3 years. In particular, we should formulate reasonable urban development plans.

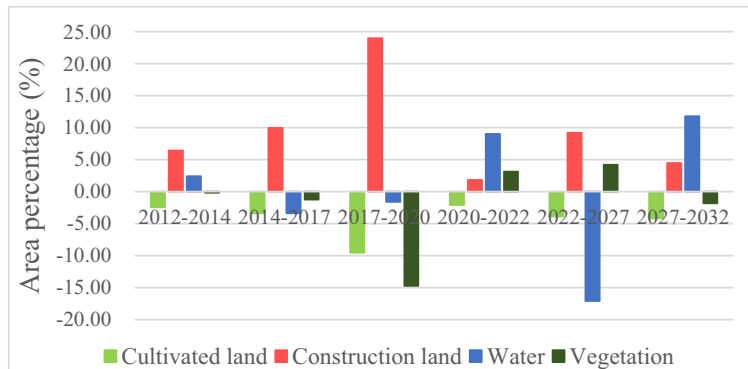
Discussion

Due to the impact of the Landsat data quality and the revisit cycle, most of the existing studies on detecting and predicting LULC change had to use a few available remotely sensed data but without considering the seasonal rhythms and phenological effects, which affect the accuracy of detection and prediction. To obtain Landsat-scale data of the ideal time period for LULC change detection and prediction, a spatiotemporal data fusion method named ESTARFM was employed to fuse Landsat images and MODIS images to generate Landsat-like data at a special time, which has been used successfully in many fields, such as urban flood

mapping (Zhang et al. 2014; Huang et al. 2016), plant phenology (Gervais et al. 2017), and winter wheat biomass estimation (Dong et al. 2016).

In this study, several simulation experiments were conducted to investigate the effect of STF on the LULC prediction accuracy. The results show that the prediction results based on the fused data are very close to the actual data. This means that when there is no Landsat data of an ideal time for the LULC prediction, we can replace them with the fused Landsat data. In addition, we also found that with a shorter inter-annual interval between the two input data, a higher prediction accuracy could be obtained. Once the Landsat-like data with a high temporal resolution were obtained by using STF, the inter-annual intervals between the two input data could be shortened. The historical LULC change in the Hefei City analysis shows a decrease of 18% in the area of cultivated land, an increase of 108.60% in the area of construction land, and a relatively stable state in areas of water and vegetation, from 1987 to 2017. With the acceleration of urbanization, cultivated land, vegetation, and areas around highways and near human settlements may be the main targets of LULC change. In future LULC predictions, we further found that the area experiences an extensive conversion to urban land cover from 1987 to 2032, eliminating approximately 33.14% of cultivated land. The rate of urban expansion peaks during 2017–2020, which will lead to the loss of cultivated land, vegetation destruction, and ecological degradation. If the land use policy remains unchanged, the major interactions between humans and the land over the next 15 years will result in a persistent decrease in the area of cultivated land (18.46%), and a continuous increase in the area of construction land (44.01%). Future plans may have to reduce the pressure on the remaining vegetation and cultivated land, and restrict

Fig. 15 Rate of gain/loss (area percentage (%)) for each land use and land cover type at different periods



the expansion of construction land. In short, the STF method successfully enhances LULC detection and prediction research.

However, it should be noted that there are some potential limitations in this study. Several uncertainty factors can affect the prediction results. The first uncertainty is with regard to the STF method. Although the prediction results from the fused data are in good agreement with the prediction results from the actual data, their prediction accuracies are slightly lower than the prediction accuracy of the actual data. On the one hand, the spatiotemporal data fusion accuracy can be affected by the input remote sensing images. Due to differences in sensor systems such as orbit parameters, bandwidth, wavelength, acquisition time, and spectral response function, there may be systematic biases in surface reflectance among different sensor remote sensing images (Wu et al. 2015). Additionally, the quality (i.e., cloud cover and differences in the MODIS viewing angles) of the input remote sensing images also affect the LULC prediction accuracy. On the other hand, the greater the landscape heterogeneity, the worse the fused effect. The second uncertainty is with regard to the classification method. Due to technical limitations, the classification process will produce subjective errors that affect the prediction accuracy of the model. The third uncertainty is with regard to the prediction model. Urban prediction is more difficult, due to its heterogeneity. In addition, factors of human activities are not considered in the process of predicting LULC data by using the CA–Markov model, which also affects the prediction accuracy. There are two main reasons for giving up these factors. First, these information are very difficult to obtain, especially for historic data in the early years. Second, the CA–Markov model is extra sensitive to the data, and it obtains satisfying results only when the input data are sufficient and true. Actually, we had tried to add party data of the road network to the model. The results show that the accuracy of the prediction is slightly reduced after adding the data of the road network. Therefore, this study did not consider these factors in the LULC prediction process. However, if the sufficient and true data of socioeconomic, policy, road network, and demographics can be obtained in the future, it is recommended to integrate the data into the CA–Markov model. In view of the fact that we mainly studied the overall trend of long-term sequences to reduce the effects of such local errors to some extent, the proposed method is therefore suitable for LULC prediction.

In the next step, techniques will be used to improve the quality of remote sensing images (such as the removal of clouds) and to further optimize the study of LULC evolutionary characteristics and prediction. This study was conducted only in Hefei; we will select multiple cities for verification and explore whether the remote sensing images acquired by spatiotemporal data fusion are applicable for the LULC prediction of watersheds, wetlands, and urban agglomerations. In addition, to improve the accuracy of the prediction results, more information, including socioeconomic, elevation, road network, policy, and demographic data, could be integrated into the prediction process (Ibrahim and Menzel 2014).

Conclusions

The STF method has been successfully used in this study for the detection and prediction of LULC, to generate same-season Landsat-like images over a period of 30 years (1987–2017). The simulation experiments show that the STF method is feasible and applicable for LULC. The fused summer Landsat-like data are used to improve the prediction accuracy of the CA–Markov model by shortening the inter-annual interval and also to obtain LULC prediction results for a specific year. The highly accurate LULC prediction results can be effectively used to analyze the consequences of future land use dynamics, which can help researchers and political decision-makers to understand the directions of dynamic changes in land use, and to adopt appropriate solutions. The techniques developed in the present study are reproducible in many other studies of land use and land cover, such as wetlands and watersheds.

Acknowledgments We thank the data providers of USGS and the International Scientific & Technical Data Mirror Site, Compute Network Information Center, Chinese Academy of Sciences. We thank Dr. Xiaolin Zhu (The Hong Kong Polytechnic University) for providing access to the ESTARFM IDL code.

Funding information This work was supported in part by the Mining environmental restoration and wetland ecological security Collaborative Innovation Center, the National Natural Science Foundation of China under Grant 41501376.

Publisher's Note Springer Nature remains neutral with regard to jurisdictional claims in published maps and institutional affiliations.

References

- Adami, M., Rudorff, B. F. T., Freitas, R. M., Aguiar, D. A., Sugawara, L. M., & Mello, M. P. (2012). Remote sensing time series to evaluate direct land use change of recent expanded sugarcane crop in Brazil. *Sustainability*, 4(4), 574–585.
- Alhamdan, M. Z., Oduor, P., Flores, A. I., Kotikot, S. M., Mugambi, R., & Ababu, J. (2017). Evaluating land cover changes in Eastern and Southern Africa from 2000 to 2010 using validated Landsat and MODIS data. *International Journal of Applied Earth Observation and Geoinformation*, 62, 8–26.
- Alqurashi, A. F., Kumar, L., & Sinha, P. (2016). Urban land cover change modelling using time-series satellite images: a case study of urban growth in five cities of Saudi Arabia. *Remote Sensing*, 8(10), 838–861.
- Ariti, A. T., Vliet, J. V., & Verburg, P. H. (2015). Land-use and land-cover changes in the central rift valley of Ethiopia: assessment of perception and adaptation of stakeholders. *Applied Geography*, 65, 28–37.
- Behera, D. (2007). Mining induced LULC change detection study using Landsat satellite data in Joda-Barbil region of Kenojhar District, Odisha, India. *International Journal of Earth Sciences & Engineering*, 10(2), 233–241.
- Blecic, I., Cecchini, A., & Trunfio, G. A. (2013). Cellular automata simulation of urban dynamics through GPGPU. *Journal of Supercomputing*, 65(2), 614–629.
- Bounoua, L., Nigro, J., Zhang, P., Thome, K., & Lachir, A. (2018). Mapping urbanization in the United States from 2001 to 2011. *Applied Geography*, 90, 123–133.
- Cammalleri, C., Anderson, M. C., Gao, F., Hain, C. R., & Kustas, W. P. (2014). Mapping daily evapotranspiration at field scales over rainfed and irrigated agricultural areas using remote sensing data fusion. *Agricultural and Forest Meteorology*, 186(10), 1–11.
- Chandra, G., Defourny, P., & Surendra, S. (2003). Land cover characterization and mapping of continental Southeast Asia using multi-resolution satellite sensor data. *International Journal of Remote Sensing*, 24(21), 4181–4196.
- Chen, L., Liu, Y., Yihe, L., Feng, X., & Fu, B. (2008). Pattern analysis in landscape ecology: progress, challenges and outlook. *Acta Ecologica Sinica*, 28(11), 5521–5531.
- Chen, L., Sun, R., & Liu, H. (2013a). Research progress of ecological environment effect in the evolution of urban landscape pattern. *Acta Ecologica Sinica*, 33(4), 1042–1050.
- Chen, Y., Li, X., Liu, X., & Ai, B. (2013b). Analyzing land-cover change and corresponding impacts on carbon budget in a fast developing sub-tropical region by integrating MODIS and Landsat TM/ETM+ images. *Applied Geography*, 45(45), 10–21.
- Derya, O. (2015). Urban growth simulation of Atakum (Samsun, Turkey) using Cellular Automata-Markov chain and multi-layer, perceptron-Markov chain models. *Remote Sensing*, 7(5), 5918–5950.
- Dong, T., Liu, J., Qian, B., Zhao, T., Jing, Q., Geng, X., Wang, J., Huffman, T., & Shang, J. (2016). Estimating winter wheat biomass by assimilating leaf area index derived from fusion of landsat-8 and modis data. *International Journal of Applied Earth Observation and Geoinformation*, 49, 63–74.
- Emelyanova, I. V., McVicar, T. R., Niel, T. G. V., Li, L. T., & Dijk, A. I. J. M. V. (2013). Assessing the accuracy of blending Landsat–MODIS surface reflectances in two landscapes with contrasting spatial and temporal dynamics: a framework for algorithm selection. *Remote Sensing of Environment*, 133(12), 193–209.
- Fu, P., & Weng, Q. (2016). A time series analysis of urbanization induced land use and land cover change and its impact on land surface temperature with Landsat imagery. *Remote Sensing of Environment*, 175, 205–214.
- Fu, X., Wang, X., & Yang, Y. J. (2018). Deriving suitability factors for CA-Markov land use simulation model based on local historical data. *Journal of Environmental Management*, 206(15), 10–19.
- Gao, F., Anderson, M. C., Zhang, X., Yang, Z., Alfieri, J. G., Kustas, W. P., & Prueger, J. H. (2017). Toward mapping crop progress at field scales through fusion of Landsat and MODIS imagery. *Remote Sensing of Environment*, 188, 9–25.
- Gao, F., Masek, J., Schwaller, M., & Hall, F. (2006). On the blending of the Landsat and MODIS surface reflectance: predicting daily Landsat surface reflectance. *IEEE Transactions on Geoscience and Remote Sensing*, 44(8), 2207–2218.
- Gashaw, T., Tulu, T., Argaw, M., & Worqlul, A. W. (2017). Evaluation and prediction of land use/land cover changes in the Andassa watershed, Blue Nile Basin, Ethiopia. *Environmental Systems Research*, 6(1), 6–17.
- Gervais, N., Buyantuev, A., Gao, F., El-Sheimy, N., Lari, Z., & Moussa, A. (2017). Modeling the effects of the urban built-up environment on plant phenology using fused satellite data. *Remote Sensing*, 9(1), 99.
- Gounaris, D., Chorianopoulos, I., & Koukoulas, S. (2018). Exploring prospective urban growth trends under different economic outlooks and land-use planning scenarios: the Case of Athens. *Applied Geography*, 90, 134–144.
- Guan, D. J., Li, H. F., Inohae, T., Su, W., Nagae, T., & Hokao, K. (2011). Modeling urban land use change by the integration of cellular automaton and Markov model. *Ecological Modelling*, 222(20–22), 3761–3772.
- Halmy, M. W. A., Gessler, P. E., Hicke, J. A., & Salem, B. B. (2015). Land use/land cover change detection and prediction in the north-western coastal desert of Egypt using Markov-CA. *Applied Geography*, 63, 101–112.
- Huang, C., Chen, Y., Zhang, S., Li, L., Shi, K., & Liu, R. (2016). Surface water mapping from Suomi NPP-VIIRS imagery at 30 m resolution via blending with Landsat data. *Remote Sensing*, 8(8), 631–645.
- Ibrahim, W. Y., & Menzel, W. P. (2014). Agricultural policy effects on land cover and land use over 30 years in Tartous, Syria, as seen in Landsat imagery. *Journal of Applied Remote Sensing*, 8(1), 319–325.
- Jafari, M. (2016). Dynamic simulation of urban expansion through a ca-markov model case study: hyrcanian region, gilan, iran. *European Journal of Remote Sensing*, 49(1), 513–529.
- Kityuttachai, K., Kumar Tripathi, N., Tipdecho, T., et al. (2013). CA-Markov analysis of constrained coastal urban growth modeling: Hua Hin Seaside City, Thailand. *Sustainability*, 5(4), 1480–1500.
- Li, X., Ling, F., Foody, G. M., Ge, Y., Zhang, Y., & Du, Y. (2017). Generating a series of fine spatial and temporal resolution

- land cover maps by fusing coarse spatial resolution remotely sensed images and fine spatial resolution land cover maps. *Remote Sensing of Environment*, 196, 293–311.
- Liu, D., Zheng, X., Zhang, C., & Wang, H. (2017a). A new temporal–spatial dynamics method of simulating land-use change. *Ecological Modelling*, 350, 1–10.
- Liu, H., & Weng, Q. (2012). Enhancing temporal resolution of satellite imagery for public health studies: a case study of West Nile virus outbreak in Los Angeles in 2007. *Remote Sensing of Environment*, 117, 57–71.
- Liu, N., Budkevitsch, P., & Treitz, P. (2017b). Examining spectral reflectance features related to Arctic percent vegetation cover: implications for hyperspectral remote sensing of arctic tundra. *Remote Sensing of Environment*, 192, 58–72.
- Mas, J. F., Kolb, M., Paegelow, M., Olmedo, M. T. C., & Houet, T. (2014). Inductive pattern-based land use/cover change models: a comparison of four software packages. *Environmental Modelling & Software*, 51(1), 94–111.
- McCarthy, M. J., Radabaugh, K. R., Moyer, R. P., & Muller-Karger, F. E. (2018). Enabling efficient, large-scale high-spatial resolution wetland mapping using satellites. *Remote Sensing of Environment*, 208, 189–201.
- Mizuuchi, H., Hiyama, T., Ohta, T., Fujioka, Y., Kambatuku, J. R., & Iijima, M. (2017). Development and evaluation of a lookup-table-based approach to data fusion for seasonal wetlands monitoring: an integrated use of AMSR series, MODIS, and Landsat. *Remote Sensing of Environment*, 199, 370–388.
- Mohammadi, A., Costelloe, J. F., & Ryu, D. (2017). Application of time series of remotely sensed normalized difference water, vegetation and moisture indices in characterizing flood dynamics of large-scale arid zone floodplains. *Remote Sensing of Environment*, 190, 70–82.
- Monseru, R. A., & Leemansb, R. (1992). Comparing global vegetation maps with the Kappa statistic. *Ecological Modelling*, 62(4), 275–293.
- Mosammam, H. M., Nia, J. T., Khani, H., Teymouri, A., & Kazemi, M. (2016). Monitoring land use change and measuring urban sprawl based on its spatial forms: the case of Qom city. *Egyptian Journal of Remote Sensing and Space Science*, 20, 103–116.
- Muller, M. R., & Middleton, J. (1994). A Markov model of land-use change dynamics in the Niagara region, Ontario, Canada. *Landscape Ecology*, 9(2), 151–157.
- Mueller, N., Lewis, A., Roberts, D., Ring, S., Melrose, R., Sixsmith, J., & Ip, A. (2016). Water observations from space: mapping surface water from 25 years of Landsat imagery across Australia. *Remote Sensing of Environment*, 174, 341–352.
- Osgouei, P. E., & Kaya, S. (2017). Analysis of land cover/use changes using Landsat 5 TM data and indices. *Environmental Monitoring and Assessment*, 189(4), 136.
- Pickard, B. R., Berkel, D. V., & Petrasova, A. (2017). Predicts of urbanization scenarios reveal trade-offs between landscape change and ecosystem services. *Landscape Ecology*, 32(3), 617–634.
- Prenzel, B. (2004). Remote sensing-based quantification of land-cover and land-use change for planning. *Progress in Planning*, 61(4), 281–299.
- Saleem, A., Corner, R., & Awange, J. (2018). On the possibility of using corona and landsat data for evaluating and mapping long-term lule: case study of iraqi kurdistan. *Applied Geography*, 90, 145–154.
- Palmate, S. S., Pandey, A., & Mishra, S. K. (2017). Modelling spatiotemporal land dynamics for a trans-boundary river basin using integrated Cellular Automata and Markov chain approach. *Applied Geography*, 82, 11–23.
- Shen, H., Huang, L., Zhang, L., Wu, P., & Zeng, C. (2016). Long-term and fine-scale satellite monitoring of the urban heat island effect by the fusion of multi-temporal and multi-sensor remote sensed data: a 26-year case study of the city of Wuhan in China. *Remote Sensing of Environment*, 172, 109–125.
- Singh, S. K., Mustak, S., Srivastava, P. K., Szabó, S., & Islam, T. (2015). Predicting spatial and decadal LULC changes through cellular automata Markov chain models using earth observation datasets and geo-information. *Environmental Processes*, 2(1), 61–78.
- Sinha, A. P., Kumar, L., & Reid, N. (2012). Three-date landsat thematic mapper composite in seasonal land-cover change identification in a mid-latitudinal region of diverse climate and land use. *Journal of Applied Remote Sensing*, 6(1), 3595.
- Walsh, S. J., Crawford, T. W., Welsh, W. F., & Crews-Meyer, K. A. (2001). A multiscale analysis of LULC and NDVI variation in Nang Rong district, northeast Thailand. *Agriculture Ecosystems & Environment*, 85(1), 47–64.
- Wang, R., Hou, h., & Murayama, Y. (2018). Scenario-based simulation of Tianjin City using a Cellular Automata–Markov model. *Sustainability*, 10, 2633. <https://doi.org/10.3390/su10082633>.
- Wu, P., Shen, H., Zhang, L., & Götsche, F. M. (2015). Integrated fusion of multi-scale polar-orbiting and geostationary satellite observations for the mapping of high spatial and temporal resolution land surface temperature. *Remote Sensing of Environment*, 156, 169–181.
- Xie, D., Gao, F., Sun, L., & Martha, A. (2018). Improving spatial-temporal data fusion by choosing optimal input image pairs. *Remote Sensing*, 10, 1142. <https://doi.org/10.3390/rs10071142>.
- Zhang, F., Zhu, X., & Liu, D. (2014). Blending MODIS and Landsat images for urban flood mapping. *International Journal of Remote Sensing*, 35(9): 3237–3253.
- Zhu, X. L., Jin, C., Feng, G., Chen, X. H., & Masek, J. G. (2010). An enhanced spatial and temporal adaptive reflectance fusion model for complex heterogeneous regions. *Remote Sensing of Environment*, 114(11), 2610–2623.